



# Using floristic gradient mapping to assess seasonal thaw depth in interior Alaska

Veronika Döpfer<sup>1,2</sup>  | Santosh Panda<sup>3</sup> | Christine Waigl<sup>3</sup> | Matthias Braun<sup>1</sup> | Hannes Feilhauer<sup>1,4,5</sup> 

<sup>1</sup>Institut für Geographie, Friedrich-Alexander Universität Erlangen-Nürnberg, Erlangen, Germany

<sup>2</sup>Department of Landscape Architecture and Environmental Planning, Technische Universität Berlin, Berlin, Germany

<sup>3</sup>Geophysical Institute, University of Alaska Fairbanks, Fairbanks, AK, USA

<sup>4</sup>Department of Earth Sciences, Freie Universität Berlin, Berlin, Germany

<sup>5</sup>Remote Sensing Centre for Earth System Research, Leipzig University & Helmholtz Centre for Environmental Research – UFZ, Leipzig, Germany

## Correspondence

Veronika Döpfer, Department of Landscape Architecture and Environmental Planning, Technische Universität Berlin, Berlin, Germany.  
Email: v.doepfer@tu-berlin.de

## Funding information

German Academic Exchange Service Program PROMOS; Bavarian State Ministry Program Fonds Hochschule International.

**Co-ordinating Editor:** Duccio Rocchini

## Abstract

**Questions:** Is it possible to map floristic gradients in heterogeneous boreal vegetation by using remote-sensing data? Does a continuous vegetation map enable the creation of a spatially continuous map of seasonal permafrost soil thaw depth?

**Location:** Bonanza Creek LTER, Fairbanks, Alaska, USA.

**Methods:** Vegetation records are subjected to an ordination to extract the predominant floristic gradient. The ordination scores are then extrapolated using Sentinel 2 imagery and a digital elevation model (DEM). As the relation between vegetation pattern and seasonal thaw depth was confirmed in this study, the spatial distribution of ordination scores is then used to predict seasonal thaw depth over the same area.

**Results:** The first dimension of the ordination space separates species corresponding to moist and cold soil conditions from species associated with well-drained soils. This floristic gradient was successfully mapped within the sampled plant communities. The extrapolated thaw depths follow the typical distribution along a topographical and geomorphological gradient for this region. Besides vegetation information also DEM derivatives show high contributions to the thaw depth modeling.

**Conclusion:** We demonstrate that floristic gradient mapping in boreal vegetation is possible. The accuracy of the thaw depth prediction model is comparable to that in previous analyses but uses a more parsimonious set of predictors, underlining the efficacy of this approach.

## KEYWORDS

boreal vegetation, ordination, permafrost, predictive mapping, remote sensing, soil-vegetation interaction

## 1 | INTRODUCTION

Permafrost, defined as ground with temperatures below 0°C for at least two consecutive years (Harris et al., 1988), covers about 22–25% of the Northern Hemisphere land area and about 80% of Alaska's surface (Jorgenson et al., 2001; Chasmer et al., 2014; Grosse et al., 2016).

It is a critical part of the global climate system, as it stores nearly twice as much carbon as the atmosphere (Vaughan et al., 2013). Permafrost stability is, however, highly affected by climatic change because its conditions and extent are coupled to surface energy and gas fluxes in the form of surface-atmosphere interactions (Vaughan et al., 2013). The intervening surface layers of these interactions are the snow

This article is a part of the Special Feature "Remote Sensing for Vegetation Science" edited by Duccio Rocchini, Hannes Feilhauer, Sebastian Schmidlein and Jana Müllerová.

This is an open access article under the terms of the Creative Commons Attribution-NonCommercial License, which permits use, distribution and reproduction in any medium, provided the original work is properly cited and is not used for commercial purposes.

© 2021 The Authors. *Applied Vegetation Science* published by John Wiley & Sons Ltd on behalf of International Association for Vegetation Science.

cover, vegetation, and the active layer (Romanovsky & Osterkamp, 1995).

The active layer is the top layer of the ground that is subject to annual thawing and freezing and underlain by permafrost (Harris et al., 1988). Active layer thickness (ALT) undergoes temporal variations, which characterize areas of permafrost aggradation or degradation (Romanovsky & Osterkamp, 1995). The annual maximum thaw depth varies with topography (Harris et al., 1988), snow cover, soil organic layer, thermal properties of the soil (Riseborough et al., 2008), and vegetation (Fisher et al., 2016).

ALT possesses a high climate forcing potential due to its regulative effect on methane and carbon emissions (Anisimov, 2007; McCalley et al., 2014; Schuur et al., 2015). Most hydrological, biological, and biochemical processes take place in this layer (Jorgenson et al., 2001; Hinkel and Nelson, 2003; Gangodagamage et al., 2014; Luo et al., 2016). A deepening of the ALT causes changes in subsurface and surface hydrology, geomorphology in the form of landslides, ground subsidence and channel development, microtopography, rooting zones and vegetation composition (Jorgenson et al., 2001; Christensen et al., 2004; Osterkamp et al., 2009; Gangodagamage et al., 2014; Grosse et al., 2016).

ALT, especially in discontinuous permafrost zones, is a critical but still uncertain parameter of climate projections, climate change impact assessment and adaptation measures (Vaughan et al., 2013; Schuur et al., 2015; Grosse et al., 2016; Chadburn et al., 2017). Currently, measurements of ALT are restricted to the point scale and to a few main sites (CALM, 2018) due to the difficult accessibility of high-latitude regions as well as time and financial resources. Approaches on modeling the spatial distribution of ALT based on correlations with air temperature exist solely for large-scale areas, which do not account for the high spatial variability of ALT (Hinkel and Nelson, 2003).

Remote sensing provides techniques to monitor the spatial heterogeneities of ALT efficiently over larger areas with a high spatial and temporal resolution. When using remote sensing for ALT estimation, indicators such as prevailing vegetation patterns are necessary (Panda et al., 2012). Several studies report interactions such as insulation, nutrient supply and soil moisture control between vegetation communities and ALT. These interactions lead to characteristic vegetation patterns along an ALT gradient (e.g. Viereck et al., 1993; Jorgenson et al., 2001; Finger et al., 2016).

Areas with bare soil or new alluvial gravel plains absorb most of the incoming solar radiation resulting in a deeper ALT and a deep rooting zone permitting a lateral percolation of precipitation. These warm and well-drained soils are preferred conditions by *Salix* spp., *Picea glauca* (white spruce), *Populus balsamifera* and *Betula papyrifera*. The mostly deciduous forests with high crown coverage create with their litter an insulating organic layer, which promotes the growth of mosses and lowers the soil temperature. With shallower ALT, trees are limited in their growth and regeneration so that the cold-soil-adapted species *Picea mariana* (black spruce) and *Larix laricina* occupy these sites (Chapin III et al., 2006). The low soil temperatures and the presence of coniferous needles decelerate the decomposition rate, forming

cold and acidic conditions. This leads to a thickening of the organic layer and further insulation of the soil (Benninghoff, 1952). As a result, tree growth and density decrease whereas lichen and moss growth increases, conserving shallow ALT and fixing available nitrogen. The increased light availability favors tundra plants like *Ledum groenlandicum*, *Vaccinium uliginosum* or *Eriophorum* spp. (Bonan & Shugart, 1989). Jorgenson et al. (2001) showed that the thawing and refreezing process leads to a conversion of tree- and shrub-dominated birch forests to herb- and sedge-dominated fen and bog.

The interactions between ALT and vegetation can be used to infer permafrost soil properties from remotely sensed data depicting the vegetation and land cover. This information could be successfully applied to map the presence and absence of near-surface permafrost with high accuracy and high spatial resolution in boreal settings (Nguyen et al., 2009; Kremer et al., 2011; Panda et al., 2012). However, no information on gradual changes of ALT is provided.

ALT degradation can be assessed via land cover characteristics such as bog landforms, wooded fens, lakes, and vegetation in boreal regions (Halsey et al., 1995; Beck et al., 2015). ALT thickness of different vegetation types was quantified but not used to assess the spatial distribution of ALT. The combination of remotely sensed land cover maps with further information such as topography or temperature showed high potential to map the spatial distribution of ALT in boreal and tundra regions (Peddle & Franklin, 1993; Nelson et al., 1997; Pastick et al., 2013). In tundra environments, the results are promising (Nelson et al., 1997; Gangodagamage et al., 2014). Nevertheless, the coarse resolution of 300 m × 300 m (Nelson et al., 1997) does not account for the influence of features smaller than 1 km<sup>2</sup> such as lakes or topographical features. Additionally, the transferability of the approach to non-tundraic regions is not yet confirmed. Peddle and Franklin (1993) derive only ALT classes within a mountainous boreal site. Pastick et al. (2013) derived high-resolution continuous ALT map in a boreal region from Landsat data and a classified land cover map. The authors report, however, uncertainties in their predictions due to inaccuracies of the input data set such as the land cover map.

To our best knowledge, all studies including vegetation cover in their permafrost or ALT analysis are based on classification methods and neglect the gradual spatial changes in both vegetation and permafrost properties.

A different approach of vegetation mapping that preserves the continuous properties of the vegetation distribution is floristic gradient mapping. This approach is based on the ordination of a plot-by-species table that describes the main gradual transitions in plant species composition. In a subsequent analysis, each pixel is assigned a position in the ordination space that is treated as indicator of its plant species composition. This ordination-based approach is optimized toward preserving the fuzzy and gradually changing characteristics in the plant species composition of the vegetation and presents a more realistic description of the vegetation continuum than hard classification (Schmidtlein et al., 2007).

Floristic gradient mapping has not been previously conducted in a continental boreal zone. This approach can reveal information on

fine-scale and transitional processes between vegetation communities avoiding uncertainties in ALT estimates due to misclassifications. In the present study, we thus address the following research questions: (a) is it possible to map floristic gradients in a heterogeneous boreal vegetation setting? (b) Does continuous vegetation mapping also enable the derivation of spatially continuous maps of the seasonal thaw depth?

## 2 | METHODS

### 2.1 | Study site

The study was implemented at four sites of the Bonanza Creek LTER network in interior Alaska (Figure 1), where long-term ALT and background environmental data are available. The areas are located in the discontinuous permafrost zone and are characterized by a continental climate including extreme temperature amplitudes, rapid inter-seasonal changes and convective rainfall in summer (Wendler & Shulski, 2009). The 30-year mean (1981–2010) of annual precipitation amounts to 276 mm, the mean annual temperature is  $-2.2^{\circ}\text{C}$  with a minimum and maximum monthly air temperature of  $-21.9^{\circ}\text{C}$  and  $17.2^{\circ}\text{C}$ , respectively (Lawrimore et al., 2011). Climate records since 1948 reveal an increase of mean annual temperature by  $1.4^{\circ}\text{C}$  between 1948 and 2006 (Wendler & Shulski, 2009).

The vegetation composition varies per site corresponding to topographic gradients, exposure to sun, fire history and permafrost

conditions. At the Bonanza Creek Experimental forest (BC) vegetation ranges from mixed to broad-leaved forest on uplands and south-facing slopes over *Picea glauca*- and *Picea mariana*-dominated foothills and north-facing slopes to *Picea mariana*-dominated woodlands in the floodplain (Viereck et al., 1993). The woodland is interrupted by several thermokarst collapse scar bogs and fens that developed over centuries. Drier hummocky terrain covered by sparse woodland re-established on areas where prior thaw occurred (Finger et al., 2016). The alluvial plain has been affected by three fires in 1983, 2001 and 2018 (Alaska Interagency Coordination Center, 2018).

The North Campus of the University of Alaska, Fairbanks (UAF) is characterized by *Picea mariana*-dominated woodlands and tussock grass in its understorey in the flat basin center. A ridge crossing this center is covered by mixed forests. Toward the edges of the basin, the terrain becomes more hummocky and dense *Picea mariana* and *Picea glauca* forests take over. As elevation increases, deciduous forests become predominant on south-facing slopes. South of Smith Lake degraded pleistocene ice-wedges (Osterkamp et al., 2000) resulted in a broad-leaved-white spruce cover, whereas eastern north slopes are covered by black and white spruce forests.

In the Caribou–Poker Creeks Research Watershed (CPCRW), deciduous forests are prominent on the southern slopes, as well, while *Picea mariana* stands dominate the northern slopes and the tussocky valley bottoms. Along the rivers *Salix* spp. and *Alnus tenuifolia* are prevalent. The north slopes consist of large rocks covered by a

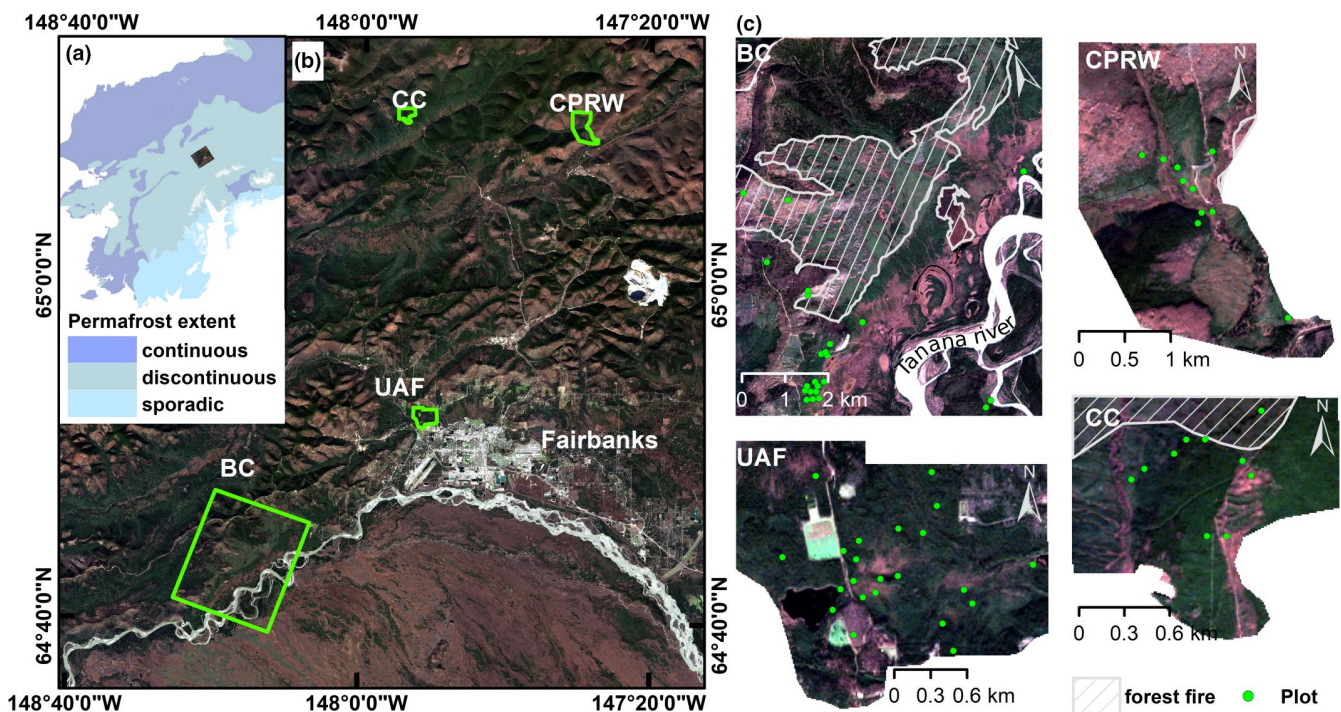


**FIGURE 1** Test site overview. (a) Permafrost extent within Alaska (Data: Brown et al., 2002); (b) general location of test sites; (c) detailed study sites with plot locations and wildfire (Data: Alaska Interagency Coordination Center, 2018) for Bonanza Creek experimental forest (BC), Caribou–Poker Creeks Research Watershed (CPCRW), University of Alaska Fairbanks North Campus (UAF) and Cushman Creek (CC). Background data: RGB composite of Sentinel 2 (2018-09-30)

20–40 cm thick lichen and moss layer. At a 2004 burn scar, *Betula neolaskana* is now established.

The prominent slopes of the Cushman Creek (CC) site are covered by a thick layer of mosses and litter. *Picea mariana* extends over the slope and basin area, while broad-leaved forest predominates on ridges. A severe fire event in 1971 was managed by the construction of a firebreak that involved the removal of the organic layer beyond the fire perimeter (Vioreck & Dyrness, 1979). Woody shrubs, mainly *Ledum groenlandicum*, *Betula nana* and *Alnus fruticosa*, with scattered *Picea mariana* trees predominate the burned areas. The different soil conditions at the fire line provide the conditions for higher-growing shrubs, mostly *Salix* spp. and *Alnus fruticosa*.

## 2.2 | Data

### 2.2.1 | Field data

In the following, we use the term seasonal thaw depth (TD) instead of ALT, because the recording of a maximum thaw depth could not be ensured during data collection. TD and species composition data were collected in June and July 2018. The main restriction for field data sampling was the access to the study site. Therefore, the plot location follows a clustered sampling approach. Main nodes correspond to areas where annual TD measurements are available and where summer fieldwork of other groups took place. The further placement of the plots had to fulfill the following two requirements: (a) a distribution along an assumed ALT gradient to assess the complete species variability associated with ALT changes, and (b) a minimum separation distance of 100 m to mitigate spatial clumping.

We sampled 67 plots in total. Based on field observations of vegetation structure and composition, we chose a plot size of 10 m × 10 m for tree species cover estimation. Within each plot, a randomly placed subplot of 5 m × 5 m was used to estimate the cover of shrubs taller than 0.5 m. Shrubs smaller than 0.5 m were sampled together with herbaceous species in an additional randomly placed 1 m × 1 m subplot, as it was difficult to estimate the species cover of shrubs smaller than 0.5 m in the 5 × 5 m area.

The coverage of all vascular species was estimated as cover fraction. For vertically overlapping species, only the coverage of the topmost species was recorded. Lichens and mosses were included in the estimate without further species differentiation within the 1 m × 1 m area. The estimates were aided by a frame used to delineate the plot area and performed by one observer to keep the observer bias homogeneous. GPS coordinates and elevation (m a.s.l.) were recorded with an average accuracy of 2.45 m in the center of the main plot.

The averaged TD per plot was measured using a steel probe at ten randomly located sites within each main vegetation plot. In hummock or tussock terrain, TD was measured equally on the top of hummocks and tussocks and in the hollows in between. When gravel or stones impeded the probe, measurements were marked and excluded.

### 2.2.2 | Remote sensing and topographical data

A time series of multispectral Sentinel-2 imagery was used as predictor data set. ESA's Sentinel-2 mission, consisting of two satellites 2A and 2B, provides a total of 13 spectral bands and offers a revisit time of less than five days. The spatial resolution varies with band, ranging from 10 m × 10 m for the blue, green, red and broad near infrared (NIR) band to 20 m × 20 m for the additional narrow RedEdge, NIR and shortwave infrared (SWIR) bands. The data were processed to top-of-atmosphere reflectance and resampled with a bilinear function to a uniform 10 m × 10 m resolution.

We selected cloud-free images over the study sites acquired on 20 Jun 2018, 22 Jul 2018 and 30 Sep 2018. The chosen dates aim for covering the most prominent phenological stages such as canopy growth, peak canopy development and senescence of the vegetation in our study sites. In addition to the spectral reflectance values, we calculated 19 spectral vegetation indexes and six texture parameters (Haralick et al., 1973) using band 8 (NIR) as additional predictor variables. These additional parameters highlight stand-specific biochemical and structural traits. The spectral indexes and texture parameters are listed in Appendix S1.

Since topography influences the permafrost distribution (Etzelmüller et al., 2001) we included a digital elevation model (DEM) in the predictor data set. We used the 5 m × 5 m pixel size Arctic DEM (Porter et al., 2018) product from Polar Geospatial Center at University of Minnesota. The Arctic DEM has missing coverage in parts of the BC site, so we used the IFSAR Alaska DEM (U.S. Geological Survey, 2013), which has also a 5 m × 5 m resolution, to fill the gaps. DEM derivatives such as roughness, slope, topographic position index, terrain ruggedness index and flow direction were derived from the DEM and added to the list of predictor variables.

## 2.3 | Analysis

### 2.3.1 | Floristic gradient extraction

We extracted the gradients inherent in the species composition of all areas by applying isometric feature mapping (isomap, Tenenbaum et al., 2000) to the Bray–Curtis distance matrix of the vegetation data. Isomap is considered an extension of classical multidimensional scaling (MDS), combining the computing advantages of the MDS with the flexibility to project non-linear manifold within the data set in a lower-dimensional space. The basis for re-mapping intrinsic structures is given by geodesic instead of linear distance metrics (Tenenbaum et al., 2000). When creating geodesic distances within a data set, it is essential to determine the nearest neighbors of a sample. We specified a radius  $\epsilon$ , which defines the maximum Bray–Curtis distance between the samples to be considered nearest neighbors. The optimum value of  $\epsilon$  was chosen iteratively. For ease of interpretation of the isomap ordination space, we used the *isomap* cluster algorithm (Schmidtlein et al., 2010) to identify characteristic species along the gradients.

### 2.3.2 | Regression modeling

To map the isomap space (i.e., to assign to each pixel in the study area a predicted position in the ordination space), the isomap axis scores to the field plots were regressed against the corresponding remotely sensed and topographic predictor values (Figure 2).

This spatial extrapolation was performed using Partial Least Squares Regression (PLSR; Wold et al., 2001). PLSR is able to deal with the high level of inter-correlation of the spectral data and topographic parameters. To improve the predictor variable selection, a jackknifing procedure was applied (Schmidtlein et al., 2012; *autopls* manual). By applying an iterative backward selection only input variables that are stable in validation, i.e., predictors of small variation during tenfold cross-validation, are considered to have a robust relationship to the dependent variable (Martens & Martens, 2000). A measure of this robustness is the significance ranging from 0 to 1. In this application a significance level  $p < 0.1$  served as threshold. The tuned model was evaluated using the tenfold cross-validation results of RMSE and  $R^2$ .

The resulting regression model was applied pixel-wise on the raster data of the predictors to achieve a mapped prediction of the ordination space position per pixel.

For the subsequent modeling and mapping of TD, predictors selected in the PLSR model for the ordination scores were excluded from the input data set. Instead, the mapped ordination scores served as additional predictor, building a new model following the afore-mentioned optimization and evaluation approach. Thereby, we used the modeled instead of the original ordination axis scores to include the variable's uncertainty in the model.

This second model was likewise applied pixel-wise on the area of interest. In order to avoid predictions in areas for which the model was not calibrated, water bodies and roads were masked out.

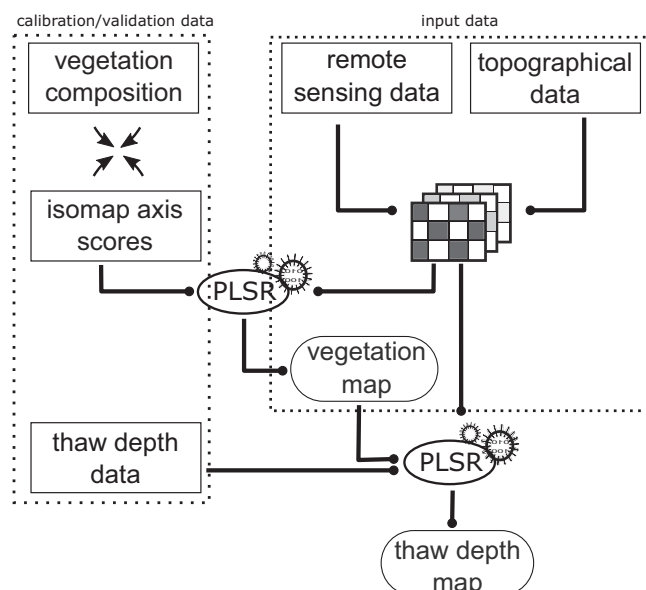


FIGURE 2 Workflow of thaw depth modeling

All analyses were conducted in the R statistical environment using the packages *vegan*, *isopam*, *autopls*, *raster*, *rgdal*, *gdalUtils* and *glcm*.

## 3 | RESULTS

For the isomap ordination, the explained variance per  $\epsilon$  as presented in Figure 3 reveals that  $\epsilon < 0.6$  leads to disconnections of the nearest-neighbor net, indicating a non-homogeneous data distribution. The best transfer of the information contained in the original data set to lower dimensions was achieved with an  $\epsilon = 0.8$ . With this setting, the first dimension explained 65% of the variation inherent to the initial vegetation data set. The second and third axis added only minor explanatory value. A correlation with measured TD was highest with the first axis ( $R^2 = 0.49$ ), as indicated by the arrow in Figure 3. The direction of the arrow highlights the direction of increasing TD values in the ordination diagram. Based on these results, only the first dimension was considered for further analysis.

The results indicate a transition from moist woodlands characterized by *Rubus chamaemorus*, *Betula nana*, *Eriophorum vaginatum*, *Chamaedaphne calyculata*, *Larix laricina* and *Oxycoccus microcarpus* with positive axis scores to *Picea mariana* forests with negative scores. Sites with scores  $\sim 0$  are occupied by coniferous forests.

With increasing axis scores, broad-leaved-dominated sites with *Populus balsamifera*, *Betula neoalaskana*, *Populus tremuloides* and *Picea glauca* in the canopy, *Viburnum edule*, *Shepherdia canadensis* and *Rosa acicularis* in the shrub and *Galium boreale*, *Linnaea borealis* and *Moehringia lateriflora* in the herbaceous layer take over.

The PLSR model for the isomap axis gained a fit of  $R^2 = 0.87$  in validation by including four latent vectors (Figure 4a). The algorithm selected four predictors of the input data set (see Appendix S1) that are all based on the red to NIR spectral regions of the early season (Figure 4b). An outlier is present at an axis score of 0.45, highly underestimating the corresponding plot's position on the isomap axis.

PLSR model fits for TD mapping are displayed in Figure 4c. The TD model included 13 predictors in five latent vectors, leading to  $RMSE_v = 13.4$  cm and  $R^2_v = 0.68$  (Figure 4d). The importance of the isomap axis scores is prominent. In addition to early and mid-season indexes, texture and DEM features are considered in the model. Despite a high  $R^2$  of 0.68 in cross-validation, the model for TD mapping shows a slight overestimation of shallow and underestimation of deep TD, as depicted in Figure 4c. Especially sites covered by dense mature coniferous forests with high moss and lichen cover on the ground tend to be highly underestimated.

The resulting mapped distribution of TD is displayed in Figure 5. A color gradient from blue to red indicates shallow to deep TD, respectively. The TD ranges from 15 cm to 120 cm, with thin TD in the basins of the study sites and deep TD on slopes and ridges. Patches of deeper TD intersect areas of shallow TD. Close to rivers and lakes, TD is deeper than in surrounding areas, which is clearly visible along the active floodplain of Tanana River at BC. At the points bars, deep TD occurs in larger areas and at a greater distance from the river bed than at cut banks.

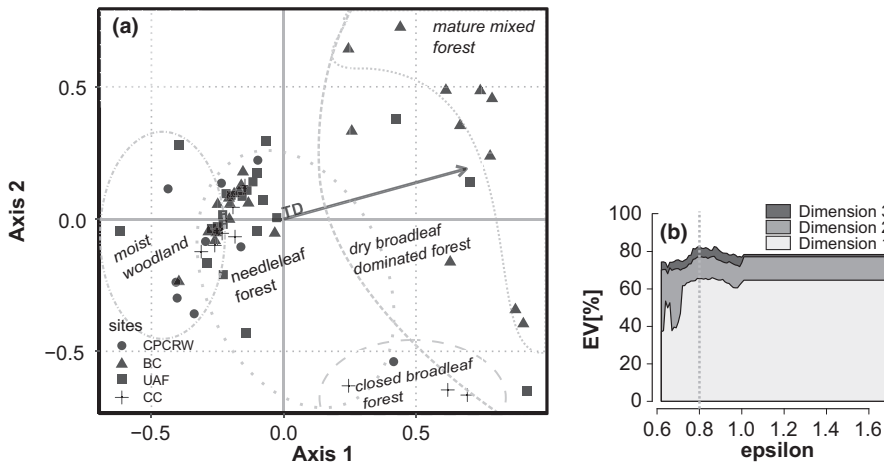


**FIGURE 3** (a) First two axes of the isomap ordination space with delineated areas showing the distribution of major vegetation types. (b) Explained variance (EV) of the original data set with varying  $\epsilon$

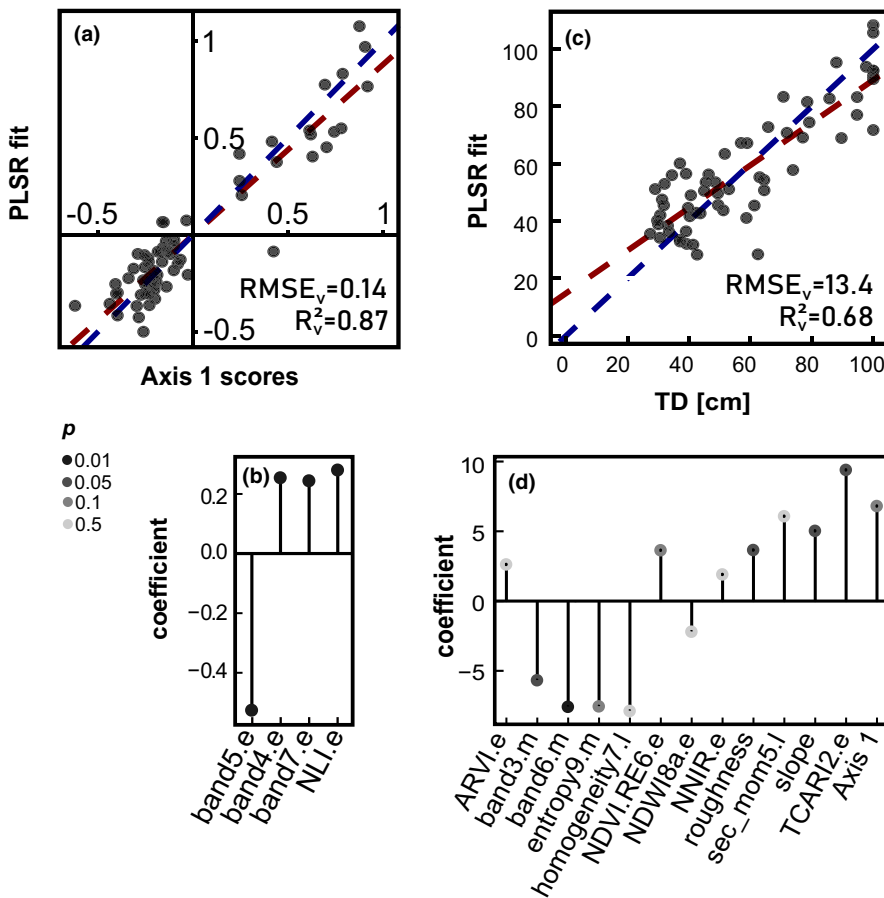


**FIGURE 4** (a) Isomap axis 1 scores and PLSR fits. (b) Coefficients included in the PLSR model for isomap score modeling. (c) Thaw depth measurements against PLSR modeled thaw depth. (d) Coefficients included in the PLSR model for thaw depth

## 4 | DISCUSSION

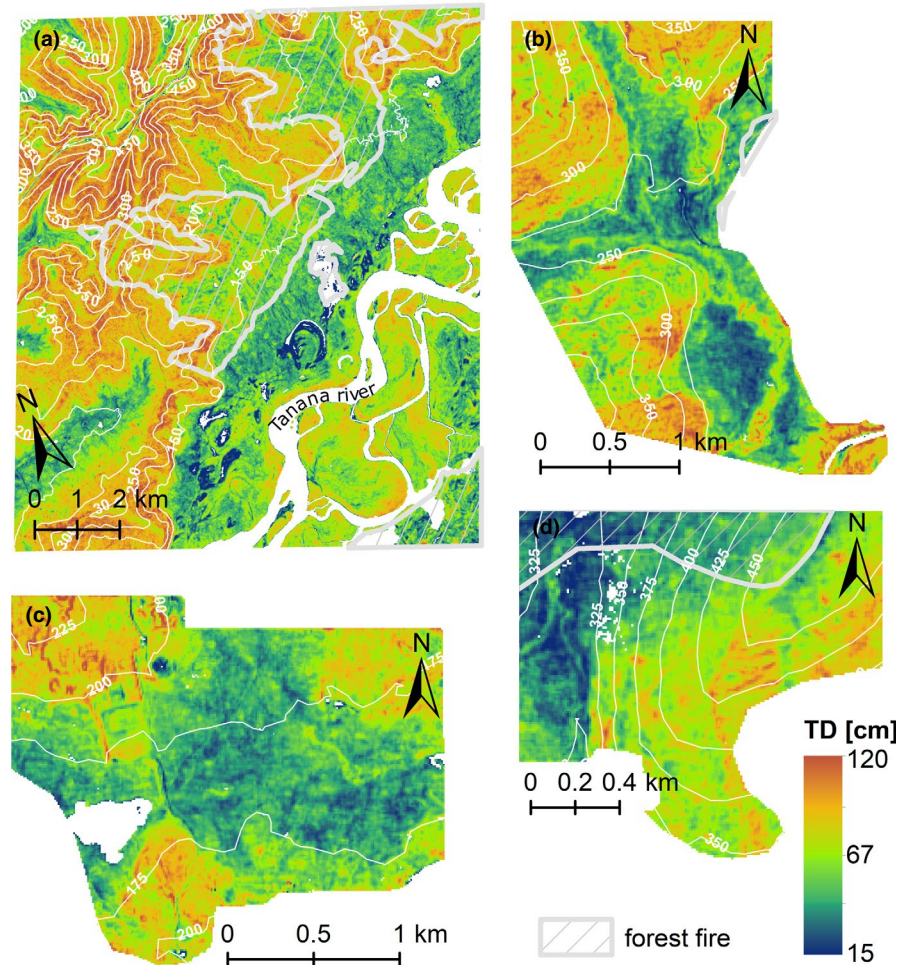
The results of the isomap analysis support the hypothesis that the main diversity in vegetation composition in our data set is driven by a TD gradient. The overall goal was to represent ALT rather than the full vegetation composition. Therefore, the representation of variation within the multidimensional vegetation data set by the first axis isomap scores is considered sufficient.

An advantage of isomap is its flexibility to find the optimal mapping for any data distribution by heuristically determining

the parameters used to define nearest neighbors. In our data set, two vegetation clusters existed which could not be connected by an isomap  $\epsilon < 0.62$ . Distances of this range are present between coniferous-dominated and broad-leaved-dominated forests (Figure 3a), revealing an unequal sampling of the transition between these vegetation compositions.

The floristic gradient extracted by the isomap ranges from cold and moist open woodlands to deciduous and mixed forest on well-drained and deep soils in high axis scores. We found that especially deciduous trees and shrubs such as *Populus tremuloides*, *Populus*

**FIGURE 5** Modeled thaw depth maps of (a) Bonanza Creek Experimental Forest, (b) Caribou–Poker Creeks Research Watershed, (c) UAF North Campus and (d) Cushman Creek



*balsamifera*, *Rosa acicularis* and *Viburnum edule* and herbaceous species *Galium boreale* and *Linnaea borealis* populate sites of deep TD. This is in accordance with the observations on vegetation communities and the corresponding soil characteristics described by Viereck et al. (1983). The authors describe that especially deep and warm soils favor poplar-dominated forests. Our analysis furthermore describes an increasing coverage of *Picea glauca* with deeper TD, which is also supported in a former analysis (Viereck et al., 1983).

For moist sites with shallow ALT, here indicated by negative axes scores, we report *Chamaedaphne calyculata*, *Oxycoccus microcarpus* and *Rubus chamaemorus* as characteristic species. Hollingsworth et al. (2006) found the same species by analyzing *Picea mariana* communities along a soil moisture gradient. We also found *Larix laricina*, *Betula. nana* and *Eriophorum vaginatum* as characteristic species for sites with very shallow TD. These species are also associated to lowest TD (Jorgenson et al., 2001).

We find shallowest TD at open woodlands, medium TD at evergreen forests and maximum values at mixed and deciduous forests. Using a vegetation classification approach, Pastick et al. (2013) showed that areas of evergreen forests are characterized by deeper ALT than mixed forests. Nevertheless, the trend in our survey is in accordance with the ALT measured in the different forest types by Panda et al. (2010).

The most prominent pattern in our spatial extrapolation of TD is the deep TD at hill ridges and shallow TD in valley bottoms. In the surrounds of Fairbanks, a high number of inversion days lead to higher temperatures of the hill ridges compared to the cooler valley bottoms (Hinzman et al., 2006). The predicted deeper TD on south-facing slopes can be explained with the higher solar radiation input. This leads to deeper ALT in these areas, while the colder shadowed northern slopes feature shallower ALT (Hinzman et al., 2006).

Areas of alluvial erosion and deposition in BC are predicted with shallower and deeper TD, respectively. At point bars permafrost develops on higher accumulation terraces when vegetation succession reaches white spruce forests. On cut bars instead developed permafrost gets eroded (e.g. Van Cleve and Viereck, 1981), leading to the observed pattern in our analysis.

The lowland areas and valley bottoms are characterized by a complex permafrost distribution and associated processes (Jorgenson et al., 2001). The complete diversity of TD and processes in the lowland area of BC cannot be assessed due to lack of ground truth data at these sites. Kremer et al. (2011) highlight this dependency of model accuracy on fieldwork intensity, which is also the case when using a gradient mapping approach (Feilhauer et al., 2014) and can be clearly seen in the shallow TD values within the not-sampled vegetation communities such as sedge–moss bog meadows, fen meadows in the collapse scar and fen areas of BC. We assume that modeled

TDs with values <15 cm are actually areas of permafrost degradation, where TDs > 100 cm occur. This assumption is supported by TD measurements in 2018 at fens and bogs by C. Dielemann and D. Rupp (pers. comm. 26 July 2018). The reason behind the shallow TD prediction is the assumed continuity of the floristic gradient toward more open and moister areas with more negative axis scores corresponding to decreasing TD. Jorgenson et al. (2001) observed that exactly these vegetation communities are associated with unfrozen ground. Wright et al. (2009) furthermore underline the enhanced thaw of permafrost with increasing soil moisture. Consequently, TD response along our vegetation scores without sampling of fen areas would be non-linear.

Another factor impacting our TD mapping accuracy is wildfire burn scars. In previously burned areas, predicted TD in this survey are shallower, indicating that the model confuses the sparse shrub-covered area with tundra vegetation associated to shallow TD areas. TD measurements in 2014 showed that deeper TD is still present at burned compared to unburned sites of the Rosie Creek fire (1983, BC; Minsley et al., 2016). The uncertain areas coincide with low or no samples at corresponding vegetation communities and TD areas, confirming the need of and dependency on intensive fieldwork (Kremer et al., 2011).

We further observed an underestimation of deep TD contrasted by an overestimation of shallow TD, a common phenomenon for predictions based on linear models. Pastick et al. (2015) report the same problem of underestimation of deep TD. According to their interpretation, such uncertainties are due to a weaker TD–vegetation interaction. Still, other studies show high accuracy in mapping near-surface permafrost distribution based on an even deeper TD threshold (Nguyen et al., 2009; Panda et al., 2010; Kremer et al., 2011). Hence, the problem is likely to rely on the calibration data for the model. Input data are restricted to a maximum TD of 100 cm but include sites of TD deeper than 100 cm. In case of a correlation of a latent vector to TD, a steady increase or decrease should lead to deeper or shallower TD. This is not possible, when setting a threshold to the model.

Our survey highlights the importance of vegetation information for modeling TD. The PLSR model for TD includes several texture metrics and spectral vegetation indices besides the modeled first isomap axis. Texture metrics have frequently been used to assess forest structures with remote sensing (St-Onge & Cavayas, 1997; Kim et al., 2009). They add vegetation characteristics to the model that are not comprehensively represented in the species compositional data. Input variables from early and midsummer contribute most to the model. Early and midsummer images are characterized by high contrast within deciduous forests, coniferous forests and open tundra vegetation (Liu et al., 2002). With increasing senescence spectral properties of tundra and deciduous forests are harder to distinguish (Nagler et al., 2000) due to increases of red reflectance (Laidler & Treitz, 2003). The importance of pigmentation is underlined by the high contribution of the TCARI2 (Transformed Chlorophyll Absorption in Reflectance Index) composed of bands of the early season in the model. Further roughness and slope are

important predictors in the PLSR model. Slopes control erosion and deposition processes. Especially depositional processes favor permafrost and thus shallower ALT at valley bottoms (Jorgenson et al., 1999).

Prior to this study, Panda et al. (2010) and Nguyen et al. (2009) successfully mapped the distribution of near-surface permafrost (within <1.6 m and 3 m drilling depth, respectively) using categorical vegetation maps and topographical parameters. Their results provide an overview of areas with near-surface permafrost. Still, no further information about the transition between the two binary classes 'near-surface permafrost present' and 'near-surface permafrost absent' can be derived. Our approach offers this information and thus enables a better insight in the gradual transitions between these binary conditions. The most prominent transitions in our results (Figure 5) concern the transition toward shallower TD with increasing distance to the cut bank and point bars as well as increasing TD with increasing elevation. Our results make theoretical assumptions of a gradually changing TD (e.g., Chapin III et al., 2006) visible. We are further able to depict changes of TD within dominant land cover classes. The latter is prominent within broad-leaved-covered areas at hill ridge and upper slope areas. TD ranges from 86 cm up to more than 110 cm. Together with the information of the associated vegetation type, this offers the possibility to detect areas prone to degradation such as the thermokarst areas and their surroundings and monitoring of hydrological or gas flux changes at small scales.

The accuracies produced here are of the same range as previous model approaches for TD in a boreal setting (Pastick et al., 2013; Pastick et al., 2015) without using external data sets such as surficial geology, land surface temperature or biomass, for example (Pastick et al., 2013). Our approach decreases the dependencies on other surveys and furthermore decreases errors due to coarse vegetation classes or wrong assignment to vegetation classes.

Modeling of TD in tundra systems lead to higher accuracies when considering the RMSE (Nelson et al., 1997; Gangodagamage et al., 2014). Gangodagamage et al. (2014) used very high-resolution spectral and LiDAR data to create a piece-wise regression model for micro-topographical subclasses. The inclusion of micro-topography is harder to assess in boreal forests, as dense tree cover precludes high-resolution DEM creation. Furthermore, TD along micro-topography shows different slope relations to macro-topography, as a comparison of Panda et al. (2010) and Gangodagamage et al. (2014) reveals.

Michaelides et al. (2018) apply a remotely sensed active layer thickness algorithm (ReSALT) which is based on the interferometric synthetic aperture radar technique to measure surface subsidence associated with the freezing and thawing of the active layer. This approach also leads to uncertainties up to 100 cm in former wildfire areas and lower  $R^2$  when comparing ReSALT TD values to ground-penetrating radar measurements. Analyses based on the freeze and thaw cycle and its associated subsidence behavior are best applied on moderately to sparsely vegetated areas (Du et al., 2019). The transferability of this approach to densely covered areas such as



boreal interior Alaska is questionable, since dense vegetation cover affects the performance of the approach. The approach presented in this study uses the vegetation composition as indicator of permafrost properties and enables insights into TD distribution at areas covered by dense forest. As forest structure and vegetation composition are still important drivers of TD conditions (e.g. Benninghoff, 1952), both LiDAR and SAR may contribute additional important information to the model (e.g. Townsend, 2002). A data fusion of radar and optical remote-sensing data could thus be a next step in more accurate TD prediction.

## 5 | CONCLUSION

We successfully mapped small-scale variations in TD in a boreal setting in interior Alaska by making use of a continuous vegetation-mapping approach. The results reveal the importance of the combined information on vegetation composition, vegetation structure and topography for model creation. The benefit of our approach is substantiated by the underlying parsimonious predictor data set leading to similar accuracies as previous studies. It also allows the observation of transition between shallow and deep TD areas including the associated vegetation composition change as an indicator. This bears special importance for infrastructure planning and adaptation and climate change-related studies such as the analysis of hydrological processes or gas fluxes.

### Acknowledgements

We would like to thank Prof. Anupma Prakash, who supported in the organization of fieldwork and related permits. We are very grateful to Glenn Juday (UAF), Danielle Rupp (MTU), Catherine Dieleman (U of G), Jamie Hollingsworth (UAF) and Karl Olson (UAF) for the insights into the functioning of the local ecosystem and for the shuttles to the study areas.

### AUTHOR CONTRIBUTIONS

VD and HF conceived of the research idea and designed the study; VD, CW and SP collected data; VD performed statistical analyses; VD, with contributions from HF drafted the initial manuscript, all authors discussed the results and contributed on writing the final manuscript.

### DATA AVAILABILITY STATEMENT

The data that support the findings of this study are available from the corresponding author upon reasonable request.

### ORCID

Veronika Döpper  <https://orcid.org/0000-0002-2927-7279>

Hannes Feilhauer  <https://orcid.org/0000-0001-5758-6303>

### REFERENCES

Alaska Interagency Coordination Center (2018) *Fire History in Alaska*. Retrieved from [https://afsmaps.blm.gov/imf\\_firehistory/imf.jsp?site=firehistory](https://afsmaps.blm.gov/imf_firehistory/imf.jsp?site=firehistory) [Accessed 16 December 2018]

- Anisimov, O.A. (2007) Potential feedback of thawing permafrost to the global climate system through methane emission. *Environmental Research Letters*, 2(4), 045016. <https://doi.org/10.1088/1748-9326/2/4/045016>
- Beck, I., Ludwig, R., Bernier, M., Lévesque, E. & Boike, J. (2015) Assessing permafrost degradation and land cover changes (1986–2009) using remote sensing data over Umiujaq, sub-arctic Québec. *Permafrost and Periglacial Processes*, 26(2), 129–141. <https://doi.org/10.1002/ppp.1839>
- Benninghoff, W.S. (1952) Interaction of vegetation and soil frost phenomena. *Arctic*, 5(1), 34–44. <https://www.jstor.org/stable/40506520>
- Bonan, G.B. & Shugart, H.H. (1989) Environmental factors and ecological processes in boreal forests. *Annual review of ecology and systematics*, 20(1), 1–28.
- Brown, J., Ferrians, O.J., Heginbottom, J.A., & Melnikov, E.S. (2002) *Circum-Arctic Map of Permafrost and Ground-Ice Conditions, Version 2*. Boulder: National Snow and Ice Data Center.
- CALM (2018) *CALM Summary Datatable*. Retrieved from <https://www2.gwu.edu/~calm/data/north.html> [Accessed 16 December 2018]
- Chadburn, S., Burke, E., Cox, P., Friedlingstein, P., Hugelius, G. & Westermann, S. (2017) An observation-based constraint on permafrost loss as a function of global warming. *Nature Climate Change*, 7(5), 340–344. <https://doi.org/10.1038/nclimate3262>
- Chapin III, F.S., Hollingsworth, T., van Murray, D.F., Viereck, L.A. & Walker, M.D. (2006) Floristic Diversity and Vegetation Distribution in the Alaskan Boreal Forest. In: F. Chapin III, M.W. Oswood, K. Cleve, L.A. Viereck, & D.L. Verbyla (Eds.), *Alaska's Changing Boreal Forest. Long-term ecological research network series* (pp. 81). –99). Oxford: Oxford University Press. ISBN: 9780195348323
- Chasmer, L., Hopkinson, C., Veness, T., Quinton, W. & Baltzer, J. (2014) A decision-tree classification for low-lying complex land cover types within the zone of discontinuous permafrost. *Remote Sensing of Environment*, 143, 73–84. <https://doi.org/10.1016/j.rse.2013.12.016>
- Christensen, T.R., Johansson, T., Åkerman, J., Mastepanov, M., Malmer, N., Friberg, T. et al. (2004) Thawing sub-arctic permafrost: Effects on vegetation and methane emissions. *Geophysical Research Letters*, 31(4), L04501. <https://doi.org/10.1029/2003GL018680>
- Du, J., Watts, J. D., Jiang, L., Lu, H., Cheng, X., Duguay, C., Farina, M., Qiu, Y., Kim, Y., Kimball, J. S., & Tarolli, P. (2019). Remote sensing of environmental changes in cold regions: methods, achievements and challenges. *Remote Sensing*, 11(16), 1952.
- Etzelmüller, B., Ødegård, R.S., Berthling, I. & Sollid, J.L. (2001) Terrain parameters and remote sensing data in the analysis of permafrost distribution and periglacial processes: principles and examples from southern Norway. *Permafrost and Periglacial Processes*, 12(1), 79–92. <https://doi.org/10.1002/ppp.384>
- Feilhauer, H., Dahlke, C., Doktor, D., Lausch, A., Schmidlein, S., Schulz, G. et al. (2014) Mapping the local variability of Natura 2000 habitats with remote sensing. *Applied Vegetation Science*, 17(4), 765–779. <https://doi.org/10.1111/avsc.12115>
- Finger, R.A., Turetsky, M.R., Kielland, K., Ruess, R.W., Mack, M.C. & Euskirchen, E.S. (2016) Effects of permafrost thaw on nitrogen availability and plant–soil interactions in a boreal Alaskan lowland. *Journal of Ecology*, 104(6), 1542–1554. <https://doi.org/10.1111/1365-2745.12639>
- Fisher, J.P., Estop-Aragonés, C., Thierry, A., Charman, D.J., Wolfe, S.A., Hartley, I.P. et al. (2016) The influence of vegetation and soil characteristics on active-layer thickness of permafrost soils in boreal forest. *Global Change Biology*, 22, 3127–3140. <https://doi.org/10.1111/gcb.13248>
- Gangodagamage, C., Rowland, J.C., Hubbard, S.S., Brumby, S.P., Liljedahl, A.K., Wainwright, H. et al. (2014) Extrapolating active layer thickness measurements across Arctic polygonal terrain using LiDAR and NDVI data sets. *Water resources research*, 50(8), 6339–6357. <https://doi.org/10.1002/2013WR014283>

- Grosse, G., Goetz, S., McGuire, A.D., Romanovsky, V.E. & Schuur, E.A.G. (2016) Changing permafrost in a warming world and feedbacks to the Earth system. *Environmental Research Letters*, 11(4), 040201. <https://doi.org/10.1088/1748-9326/11/4/040201>
- Halsey, L.A., Vitt, D.H. & Zoltai, S.C. (1995) Disequilibrium response of permafrost in boreal continental western Canada to climate change. *Climatic Change*, 30(1), 57–73. <https://doi.org/10.1007/BF01093225>
- Haralick, R.M., Shanmugam, K. & Dinstein, I. (1973) Textural features for image classification. *IEEE Transactions on systems, man, and cybernetics*, 6, 610–621. <https://doi.org/10.1109/TSMC.1973.4309314>
- Harris, S.A., French, H.M., Heginbottom, J.A., Johnston, G.H., Ladanyi, B., Sego, D.C. & et al. (1988) *Glossary of permafrost and related ground-ice terms*. Technical Memorandum No. 142. Ottawa, Canada: National Research Council of Canada.
- Hinkel, K. M., & Nelson, F. E. (2003). Spatial and temporal patterns of active layer thickness at Circumpolar Active Layer Monitoring (CALM) sites in northern Alaska, 1995–2000. *Journal of Geophysical Research: Atmospheres*, 108(D2), 8168. <https://doi.org/10.1029/2001JD000927>
- Hinzman, L.D., Viereck, L.A., Adams, P.C., Romanovsky, V.E., Yoshikawa, K. (2006) Climate and Permafrost Dynamics of the Alaskan Boreal Forest. In: F. Chapin III, M.W. Oswood, K. Cleve, L.A. Viereck, & D.L. Verbyla (Eds.) *Verbyla Alaska's Changing Boreal Forest. Long-term ecological research network series* (pp. 39–61). Oxford: Oxford University Press. ISBN: 9780195348323.
- Hollingsworth, T., Walker, M.D., Chapin, F.S. & Parsons, A.D. (2006) Scale-dependent environmental controls over species composition in Alaskan black spruce communities. *Canadian Journal of Forest Research*, 36(7), 1781–1796. <https://doi.org/10.1139/x06-061>
- Ji, L., Wylie, B.K., Nossor, D.R., Peterson, B., Waldrop, M.P., McFarland, J.W. et al. (2012) Estimating aboveground biomass in interior Alaska with Landsat data and field measurements. *International Journal of Applied Earth Observation and Geoinformation* 18, 451–461. <https://doi.org/10.1016/j.jag.2012.03.019>
- Jin, S., Yang, L., Zhu, Z. & Homer, C. (2017) A land cover change detection and classification protocol for updating Alaska NLCD 2001 to 2011. *Remote Sensing of Environment*, 195, 44–55. <https://doi.org/10.1016/j.rse.2017.04.021>
- Jorgenson, M., Racine, C.H., Walters, J.C. & Osterkamp, T.E. (2001) Permafrost degradation and ecological changes associated with a warming climate in central Alaska. *Climatic change*, 48(4), 551–579. <https://doi.org/10.1023/A:1005667424292>
- Jorgenson, M.T., Roth, J.E., Reynolds, M., Smith, M.D., Lentz, W., Zusi-Cobb, A. et al. (1999) *An ecological land survey for Fort Wainwright, Alaska*. Hanover NH: U.S. Army Corps of Engineers Cold Regions Research and Engineering Laboratory (CRREL), 99-9.
- Kim, M., Madden, M. & Warner, T.A. (2009) Forest type mapping using object-specific texture measures from multispectral ikonos imagery. *Photogrammetric Engineering & Remote Sensing*, 75(7), 819–829. <https://doi.org/10.14358/PERS.75.7.819>
- Kremer, M., Lewkowicz, A.G., Bonnaventure, P.P. & Sawada, M.C. (2011) Utility of classification and regression tree analyses and vegetation in mountain permafrost models, Yukon, Canada. *Permafrost and Periglacial Processes*, 22(2), 163–178. <https://doi.org/10.1002/ppp.719>
- Laidler, G.J. & Treitz, P. (2003) Biophysical remote sensing of arctic environments. *Progress in Physical Geography*, 27(1), 44–68. <https://doi.org/10.1191/0309133303pp358ra>
- Lawrimore, J.H., Menne, M.J., Gleason, B.E., Williams, C.N., Wuertz, D.B., Vose, R.S. & Rennie, J. (2011) Global Historical Climatology Network - Monthly (GHCN-M), Version 3. [GHCND:USW00026411]. NOAA National Centers for Environmental Information. 2020, 10.7289/V5X34VDR [Accessed 30 May].
- Liu, Q.J., Takamura, T., Takeuchi, N. & Shao, G. (2002) Mapping of boreal vegetation of a temperate mountain in China by multitemporal Landsat TM imagery. *International Journal of Remote Sensing*, 23(17), 3385–3405. <https://doi.org/10.1080/01431160110076171>
- Luo, D., Wu, Q., Jin, H., Marchenko, S.S., Lü, L. & Gaom, S. (2016) Recent changes in the active layer thickness across the northern Hemisphere. *Environmental Earth Sciences*, 75(7), 555. <https://doi.org/10.1007/s12665-015-5229-2>
- Martens, H. & Martens, M. (2000) Modified jack-knife estimation of parameter uncertainty in bilinear modelling by partial least squares regression (PLSR). *Food Quality and Preference*, 11, 5–16. [https://doi.org/10.1016/S0950-3293\(99\)00039-7](https://doi.org/10.1016/S0950-3293(99)00039-7)
- McCalley, C., Woodcroft, B., Hodgkins, S., Wehr, R.A., Kim, E.-H., Mondav, R. et al. (2014) Methane dynamics regulated by microbial community response to permafrost thaw. *Nature*, 514(7523), 478. <https://doi.org/10.1038/nature13798>
- Michaelides, R., Schaefer, K., Zebker, H.A., Parsekian, A., Liu, L., Chen, J. et al. (2018) Inference of the impact of wildfire on permafrost and active layer thickness in a discontinuous permafrost region using the remotely sensed active layer thickness (ReSALT) algorithm. *Environmental Research Letters*, 14(3), 035007. <https://doi.org/10.1088/1748-9326/aaf932>
- Minsley, B.J., Pastick, N.J., Wylie, B.K., Brown, D.R.N. & Andy Kass, M. (2016) Evidence for non uniform permafrost degradation after fire in boreal landscapes. *Journal of Geophysical Research: Earth Surface*, 121(2), 320–335. <https://doi.org/10.1002/2015JF003781>
- Nagler, P., Daughtry, C. & Goward, S. (2000) Plant litter and soil reflectance. *Remote Sensing of Environment*, 71(2), 207–215. [https://doi.org/10.1016/S0034-4257\(99\)00082-6](https://doi.org/10.1016/S0034-4257(99)00082-6)
- Nelson, F., Shiklomanov, N.I., Mueller, G.R., Hinkel, K.M., Walker, D.A. & Bockheim, J.G. (1997) Estimating active-layer thickness over a large region: Kuparuk River basin, Alaska, USA. *Arctic and Alpine Research*, 29(4), 367–378. <https://doi.org/10.1080/00040851.1997.12003258>
- Nguyen, T.-N., Burn, C.R., King, D.J. & Smith, S.L. (2009) Estimating the extent of near-surface permafrost using remote sensing, Mackenzie Delta. *Northwest Territories. Permafrost and Periglacial Processes*, 20(2), 141–153. <https://doi.org/10.1002/ppp.637>
- Osterkamp, T.E., Jorgenson, M.T., Schuur, E.A.G., Shur, Y.L., Kanevskiy, M.Z., Vogel, J.G. et al. (2009) Physical and ecological changes associated with warming permafrost and thermokarst in interior Alaska. *Permafrost and Periglacial Processes*, 20(3), 235–256. <https://doi.org/10.1002/ppp.656>
- Osterkamp, T., Viereck, L., Shur, Y., Jorgenson, M.T., Racine, C., Doyle, A. et al. (2000) Observations of thermokarst and its impact on boreal forests in Alaska, USA. *Arctic, Antarctic, and Alpine Research*, 32(3), 303–315. <https://doi.org/10.1080/15230430.2000.12003368>
- Panda, S.K., Prakash, A., Solie, D.N., Romanovsky, V.E. & Jorgenson, M.T. (2010) Remote sensing and field-based mapping of permafrost distribution along the Alaska Highway corridor, interior Alaska. *Permafrost and Periglacial Processes*, 21(3), 271–281. <https://doi.org/10.1002/ppp.686>
- Panda, S.K., Prakash, A., Jorgenson, M.T. & Solie, D.N. (2012) Near-surface permafrost distribution mapping using logistic regression and remote sensing in interior Alaska. *GIScience & Remote Sensing*, 49(3), 346–363. <https://doi.org/10.2747/1548-1603.49.3.346>
- Pastick, N.J., Jorgenson, M.T., Wylie, B.K., Minsley, B.J., Ji, L., Walvoord, M.A. et al. (2013) Extending airborne electromagnetic surveys for regional active layer and permafrost mapping with remote sensing and ancillary data, Yukon Flats Ecoregion, Central Alaska. *Permafrost and Periglacial Processes*, 24(3), 184–199. <https://doi.org/10.1002/ppp.1775>
- Pastick, N.J., Jorgenson, M.T., Wylie, B.K., Nield, S.J., Johnson, K.D. & Finley, A.O. (2015) Distribution of near-surface permafrost in Alaska: Estimates of present and future conditions. *Remote Sensing of Environment*, 168, 301–315. <https://doi.org/10.1016/j.rse.2015.07.019>

- Peddle, D.R. & Franklin, S.E. (1993) Classification of permafrost active layer depth from remotely sensed and topographic evidence. *Remote Sensing of Environment*, 44(1), 67–80. [https://doi.org/10.1016/0034-4257\(93\)90103-5](https://doi.org/10.1016/0034-4257(93)90103-5)
- Porter, C., Morin, P., Howat, I., Noh, M.-J., Bates, B., Peterman, K. et al. (2018) ArcticDEM. *Harvard Dataverse*, V1. <https://doi.org/10.7910/DVN/OHHUKH> [Accessed 21 August, 2018]
- Qi, J., Chehbouni, A., Huete, A.R., Kerr, Y.H. & Sorooshian, S. (1994) A modified soil adjusted vegetation index. *Remote sensing of environment*, 48(2), 119–126. [https://doi.org/10.1016/0034-4257\(94\)90134-1](https://doi.org/10.1016/0034-4257(94)90134-1)
- Riseborough, D., Shiklomanov, N., Etzelmüller, B., Gruber, S. & Marchenko, S. (2008) Recent advances in permafrost modelling. *Permafrost Periglacial Processes*, 19, 137–156. <https://doi.org/10.1002/ppp.615>
- Romanovsky, V. & Osterkamp, T. (1995) Interannual variations of the thermal regime of the active layer and near-surface permafrost in northern Alaska. *Permafrost and Periglacial Processes*, 6(4), 313–335. <https://doi.org/10.1002/ppp.3430060404>
- Schmidtlein, S., Feilhauer, H. & Bruelheide, H. (2012) Mapping plant strategy types using remote sensing. *Journal of Vegetation Science*, 23(3), 395–405. <https://doi.org/10.1111/j.1654-1103.2011.01370.x>
- Schmidtlein, S., Tichý, L., Feilhauer, H. & Faude, U. (2010) A brute-force approach to vegetation classification. *Journal of Vegetation Science*, 21(6), 1162–1171. <https://doi.org/10.1111/j.1654-1103.2010.01221.x>
- Schmidtlein, S., Zimmermann, P., Schüpferling, R. & Weiß, C. (2007) Mapping the floristic continuum: Ordination space position estimated from imaging spectroscopy. *Journal of Vegetation Science*, 18(1), 131–140. <https://doi.org/10.1111/j.1654-1103.2007.tb02523.x>
- Schuur, E.A., McGuire, A., Schädel, C., Grosse, G., Harden, J.W., Hayes, D.J. et al. (2015) Climate change and the permafrost carbon feedback. *Nature*, 520, 171–179. <https://doi.org/10.1038/nature14338>
- St-Onge, B.A. & Cavayas, F. (1997) Automated forest structure mapping from high resolution imagery based on directional semivariogram estimates. *Remote Sensing of Environment*, 61(1), 82–95. [https://doi.org/10.1016/S0034-4257\(96\)00242-8](https://doi.org/10.1016/S0034-4257(96)00242-8)
- Tenenbaum, J.B., Silva, V.D. & Langford, J.C. (2000) A global geometric framework for nonlinear dimensionality reduction. *Science*, 290(5500), 2319–2323. <https://doi.org/10.1126/science.290.5500.2319>
- Townsend, P.A. (2002) Estimating forest structure in wetlands using multitemporal SAR. *Remote Sensing of Environment*, 79(2–3), 288–304. [https://doi.org/10.1016/S0034-4257\(01\)00280-2](https://doi.org/10.1016/S0034-4257(01)00280-2)
- U.S. Geological Survey. (2013) Interferometric Synthetic Aperture Radar (IFSAR) Alaska. <https://earthexplorer.usgs.gov>
- Van Cleve, K., & Viereck, L. A. (1981). Forest succession in relation to nutrient cycling in the boreal forest of Alaska. In *Forest succession* (pp. 185–211). New York, NY: Springer.
- Vaughan, D.G., Comiso, J.C., Allison, I., Carrasco, J., Kaser, G., Kwok, R. et al. (2013) Observations: Cryosphere. In: Stocker, T.F., Qin, D., Plattner, G.-K., Tignor, M., Allen, S.K. and Boschung, J. (Eds.) *Climate Change 2013: The Physical Science Basis. Contribution of Working Group I to the Fifth Assessment Report of the Intergovernmental Panel on Climate Change*. Cambridge: Cambridge University Press, pp. 317–382.
- Viereck, L. & Dyrness, C. (1979) Ecological effects of the Wickersham Dome fire near Fairbanks, Alaska. In: US Department of Agriculture, Forest Service, Pacific Northwest Research Station (Eds), *General Technical Report*, 90. Portland.
- Viereck, L.A., Dyrness, C.T., Cleve, K.V. & Foote, M.J. (1983) Vegetation, soils, and forest productivity in selected forest types in interior Alaska. *Canadian Journal of Forest Research*, 13(5), 703–720.
- Viereck, L., Dyrness, C. & Foote, M. (1993) An overview of the vegetation and soils of the floodplain ecosystems of the Tanana River, interior Alaska. *Canadian Journal of Forest Research*, 23(5), 889–898. <https://doi.org/10.1139/x93-117>
- Wendler, G. & Shulski, M. (2009) A century of climate change for Fairbanks, Alaska. *Arctic*, 62(3), 295–300. [www.jstor.org/stable/40513307](http://www.jstor.org/stable/40513307).
- Wright, N., Hayashi, M. & Quinton, W.L. (2009) Spatial and temporal variations in active layer thawing and their implication on runoff generation in peat-covered permafrost terrain. *Water Resources Research*, 45(5), W05414. <https://doi.org/10.1029/2008WR006880>
- Wold, S., Sjöström, M. & Eriksson, L. (2001) PLS-regression: a basic tool of chemometrics. *Chemometrics and Intelligent Laboratory Systems*, 58(2), 109–130. [https://doi.org/10.1016/S0169-7439\(01\)00155-1](https://doi.org/10.1016/S0169-7439(01)00155-1)

## SUPPORTING INFORMATION

Additional supporting information may be found online in the Supporting Information section.

**Appendix S1.** List of predictor variables for modeling isomap scores and seasonal thaw depth.

**How to cite this article:** Döppler V, Panda S, Waigl C, Braun M, Feilhauer H. Using floristic gradient mapping to assess seasonal thaw depth in interior Alaska. *Appl Veg Sci*. 2021;24:e12561. <https://doi.org/10.1111/avsc.12561>